AIP | Journal of Applied Physics

Electronic, structural, and magnetic effects of 3d transition metals in hematite

Muhammad N. Huda, Aron Walsh, Yanfa Yan, Su-Huai Wei, and Mowafak M. Al-Jassim

Citation: J. Appl. Phys. **107**, 123712 (2010); doi: 10.1063/1.3432736
View online: http://dx.doi.org/10.1063/1.3432736
View Table of Contents: http://jap.aip.org/resource/1/JAPIAU/v107/i12
Published by the American Institute of Physics.

Electronic, structural, and magnetic effects of 3*d* transition metals in hematite

Muhammad N. Huda,[a] Aron Walsh,[b] Yanfa Yan,[c] Su-Huai Wei, and Mowafak M. Al-Jassim
National Renewable Energy Laboratory, Golden, Colorado 80401, USA

(Received 23 March 2010; accepted 27 April 2010; published online 21 June 2010)

We present a density-functional theory study on the electronic structure of pure and 3*d* transition metal (TM) (Sc, Ti, Cr, Mn, and Ni) incorporated α-Fe_2O_3. We find that the incorporation of 3*d* TMs in α-Fe_2O_3 has two main effects such as: (1) the valence and conduction band edges are modified. In particular, the incorporation of Ti provides electron carriers and reduces the electron effective mass, which will improve the electrical conductivity of α-Fe_2O_3. (2) The unit cell volume changes systematically such as: the incorporation of Sc increases the volume, whereas the incorporation of Ti, Cr, Mn, and Ni reduces the volume monotonically, which can affect the hopping probability of localized charge carriers (polarons). We discuss the importance of these results in terms of the utilization of hematite as a visible-light photocatalyst. © *2010 American Institute of Physics*. [doi:10.1063/1.3432736]

I. INTRODUCTION

Semiconductor materials for economical photoelectrochemical (PEC) production of hydrogen using solar energy have attracted great attention since the demonstration of water splitting using a TiO_2 photoanode illuminated with ultraviolet light almost forty years ago by Fujishima and Honda.[1] To realize low-cost PEC production of hydrogen, the semiconductor materials must be abundant, inexpensive, stable in aqueous solutions, and yet have high solar-to-hydrogen conversion efficiency. However, so far, no single material has been found that meets all these criteria, even though more than 200 semiconducting materials have been studied as potential photocatalysts.[2,3]

Hematite (α-Fe_2O_3) has been considered a promising material that may potentially meet the above-mentioned criteria because of the following advantages:[2,4] α-Fe_2O_3 is inexpensive, abundant, nontoxic, and stable in most alkaline electrolytes. It has a bandgap of 2.2 eV, which is capable of absorbing roughly 40% of the solar spectrum, leading to a maximum theoretical solar-to-hydrogen conversion efficiency of about 13% under AM1.5 illumination (the global standard spectral irradiance). Its valence band edge position matches the H_2O/O_2 oxidation potential for efficient oxygen evolution, and its conduction band edge position is just slightly lower than the hydrogen reduction potential. However, despite these favorable characteristics, the maximum experimental solar-to-chemical efficiency reported in the literature for hematite is less than 3%.[5] The extremely low electrical conductivity and the indirect bandgap (weak optical absorption) are the two most critical factors that limit the PEC performance of α-Fe_2O_3.[6,7]

The PEC performance of α-Fe_2O_3 has been shown to be affected dramatically by the incorporation of transition metal (TM) and post-TM elements at concentrations of several percent.[8–15] The incorporation of 3*d* metals has demonstrated particularly interesting effects. For example, the incorporation of Ti and Cr in α-Fe_2O_3 has led to significantly enhanced photocurrents.[10,12] The incorporation of impurities may affect the properties of synthesized materials in many ways, such as structure, morphology, electronic nature, and catalytic behavior. In this paper, we study how the electronic structure, magnetic properties, and crystal volume of α-Fe_2O_3 can be changed by the incorporation of some 3*d* TMs (Sc, Ti, Cr, Mn, and Ni) using the first-principles density-functional theory (DFT). We find that the conduction band edge of α-Fe_2O_3 is highly localized, leading to a heavy electron effective mass and, therefore, very low electron conductivity. This is consistent with the fact that α-Fe_2O_3 has achieved solar-to-hydrogen conversion efficiencies well below its theoretical limit.

The incorporation of 3*d* TM in α-Fe_2O_3 has two main effects such as: (1) the valence and conduction band edges are modified. In particular, the incorporation of Ti and Cr reduces the electron effective mass, which would improve the electron conductivity of α-Fe_2O_3 and hence explain why the incorporation of Ti and Cr in α-Fe_2O_3 has led to significantly enhanced photocurrents. (2) The incorporation of Sc increases the unit cell volume, whereas, the incorporation of Ti, Cr, Mn, and Ni reduces the volume monotonically. As the transport properties of α-Fe_2O_3 are limited by small polaron (trapped charge carrier) mobility, the volume change may also affect the electrical conductivity through altering the hopping probabilities.

[a]Present address: Department of Physics, University of Texas at Arlington, Arlington, Texas. Electronic mail: huda@uta.edu.
[b]Present address: University College London, Department of Chemistry, Materials Chemistry, London WC1H 0AJ, United Kingdom. Electronic mail: a.walsh@ucl.ac.uk.
[c]Author to whom correspondence should be addressed. Electronic mail: yanfa.yan@nrel.gov.

II. METHOD

We have employed DFT to calculate the electronic properties of the bulk and defective α-Fe_2O_3 structures. The calculations were performed using the local spin density approximation[16] to DFT with the projector augmented wave (PAW) method[17,18] within the Vienna *ab initio* simulation package (VASP 4.6.21).[19,20] A well-converged plane-wave cutoff energy of 500 eV was used, and the ion positions and volumes of the supercells were always relaxed by minimizing the force on each of the atoms and stress on the cell. For α-Fe_2O_3 because Fe d bands are strongly correlated, we adopted the LSDA+U (Ref. 21) approach with U=5.5 eV for the Fe d and dopant 3d bands. We have tested with several U-values and their implication on the volume of the cell: U=5.5 eV provides a reasonable description of the bandgap and a better lattice-constant compared to experiment; larger U values give rise to too small a cell volume due to the higher localization of the Fe d electrons. Bandyopadhyay *et al.*[22] employing a similar methodology found that U=5 eV provides a good description of the bandgap and magnetic moment of Fe, while higher values of U gave a larger bandgap than the experimental one, almost by 0.4 eV. Additional studies have shown before (with VASP, Ref. 23), that at around U=5 eV, the Fe–Fe distance approaches the experimental value, which is important, as the polaron conductivity in α-Fe_2O_3 depends on this distance. On the other hand, without the Coulomb U correction, the magnetic ordering of α-Fe_2O_3 is not well described and the bandgap is highly underestimated. With U, the bandgap (separation of the occupied and unoccupied Kohn–Sham eigenvalues) is found to be 1.72 eV, close to the experimental bandgap of 2.2 eV.

The primitive unit cell of α-Fe_2O_3 has rhombohedral symmetry (the corundum structure, space group 167). Each Fe is coordinated by six oxygen atoms in a distorted octahedron and each O has four Fe neighbors. To accommodate the layered antiferromagnetic (AFM) ordering observed in α-Fe_2O_3 at low temperature, the hexagonal lattice containing three primitive cells (12 Fe atoms and 18 O atoms) was used in this study. In the hexagonal lattice (Fig. 1) each layer of Fe atoms is separated by a plane of O atoms. The coupling between the Fe atoms within each layer is ferromagnetic, whereas, the coupling between the layers is AFM below 960 K.[24] This particular magnetic configuration plays an important role in determining the conduction properties of this material. For 3d TM incorporation, one of the six spin-down Fe atoms are substituted by a 3d TM atom, which corresponds to 8.3% substitution at the Fe site. The volume and internal positions of the defective cell were fully relaxed to release the external pressure, simulating isobaric defect formation above the impurity limit.

III. RESULTS AND DISCUSSION

The Fe ($4s^2 3d^6$) atom has a formal Fe^{3+} (d^5) ionization state in α-Fe_2O_3, which is in a high spin magnetic configuration giving a nominal local magnetic moment of 5 μ_B per ion but these spins are ordered to give an overall type II AFM ground state (Fig. 1). Figure 2(a) shows the electronic band structure, and Fig. 2(b) contains the calculated partial

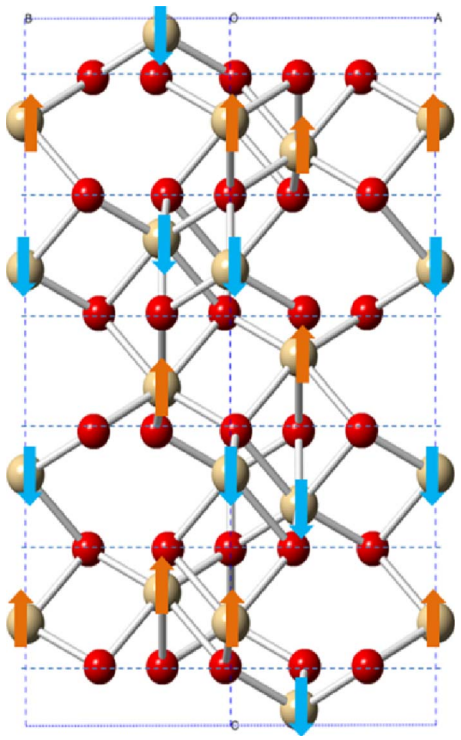

FIG. 1. (Color online) Hexagonal Fe_2O_3 lattice with AFM spin arrangements indicated by up and down arrows at the Fe sites. Small and large balls are oxygen and iron atoms, respectively.

(ion and angular momentum projected) density of states (p-DOS) plot for α-Fe_2O_3. The valence band maximum (VBM) has mostly O p and Fe d character and the conduction band minimum (CBM) has mostly minority-spin Fe d character. Due to these orbital features, the band structure of α-Fe_2O_3 has an almost dispersionless CBM between the M and K points in the first Brillouin zone. This indicates that pure α-Fe_2O_3 has extremely heavy carrier effective masses, which will result in low mobility for the electrons. This is consistent with the fact that the conducting mechanism in α-Fe_2O_3 is polaronic (localized electron carriers), which has been previously modeled using Marcus' theory,[25] and is one of the main reasons why low solar-to-hydrogen conversion efficiency has been obtained with α-Fe_2O_3 despite its favorable bandgap. The lower part of the conduction band between Γ and A is also very flat and at higher energy compared to the CBM. It implies that interlayer conduction along the z-direction will be severely suppressed; the conductivity is known to be highly anisotropic, being significantly higher within the layers in the a-b plane.[25] Thus, electron conduction in α-Fe_2O_3 essentially occurs along the same layers where all the Fe atoms have the same magnetic moment. On the other hand, the VBM, which lies between M and K points, has some dispersion feature due to the favorable p-d hybridization between the O p and Fe d states. Therefore, holes have a lower effective mass, which would suggest a higher mobility compared to electrons, neglecting the nature of their polaronic distortion.

We now discuss how the electronic structure may be modified by incorporation of 3d TMs. We have considered the 3d TMs of Sc, Ti, Cr, Mn, and Ni. From Sc to Ni, the

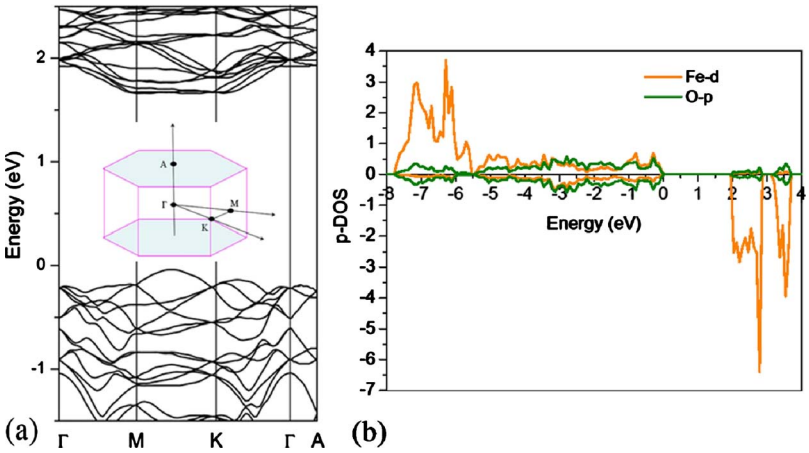

FIG. 2. (Color online) (a) Calculated electronic band structure and (b) p-DOS plot for pure α-Fe_2O_3. The inset in Fig. 2(a) shows the first Brillouin zone and special points used for the band structure plot. The highest occupied state is set to 0 eV.

number of *d* electrons increases, whereas, the electronegativity increases and the *d* orbital becomes more localized.[26] As a result, the effect of incorporation of these 3*d* TMs in α-Fe_2O_3 can be explained following these trends.

α-Fe_2O_3:Sc. Sc ($4s^2 3d^1$) is isovalent to Fe: a Sc^{3+} (d^0) ion at an Fe^{3+} site formally loses its three valence electrons, which results in a closed shell electronic configuration. The total magnetic moment of the defective Fe_2O_3 cell is derived from an unpaired Fe^{3+} (d^5) ion giving 5 μ_B. Figure 3 shows the calculated band structure of α-Fe_2O_3:Sc for spin-up (left panel) and spin-down (right panel) states. The bandgaps are 1.65 eV and 1.79 eV for spin-up and spin-down bands, respectively, which can be compared to the calculated bandgap for pure α-Fe_2O_3 (1.72 eV). There is almost no change in the features of the CBM because it still has Fe 3*d* character and the Sc 3*d* bands are positioned at higher energy. This means that the heavy effective mass for electrons remains unchanged. Therefore, incorporation of Sc into α-Fe_2O_3 may reduce the bandgap slightly, thus enhancing photon absorption; but it would not affect the intrinsic electronic conductivity of α-Fe_2O_3.

α-Fe_2O_3:Ti. Ti ($4s^2 3d^2$) has four valence electrons and favors a 4+ charge state. Substitution of the Ti^{4+} (d^0) ion at an Fe^{3+} site results in one conduction band electron. Figure 4 shows the calculated band structure of α-Fe_2O_3:Ti for spin-up (left panel) and spin down (right panel). From the band structure, we see that the conduction band is partially occupied and the CBM of the α-Fe_2O_3:Ti system is heavily modified by Ti *s* and *d* orbitals. In this case, the CBM becomes more dispersive than that of the pristine α-Fe_2O_3, indicating that alloying with Ti may reduce the effective mass for electrons, and the additional conduction electrons (*n*-type charge carriers) will further aid electron transport rates. The delocalization of the CBM state is further confirmed by the fact that the local magnetic moment of Ti is less than −0.1 μ_B, although the total magnetic moment of the cell is 4 μ_B. This is because the conduction band of α-Fe_2O_3 is lower than that of TiO_2, i.e., Fe_2O_3 has a larger electron affinity.[27] The surplus electron will not be trapped on the Ti impurity center to form a Ti^{3+} (d^1) species but will be donated to the Fe host. The spin-up CBM does not show much change from that of the pure α-Fe_2O_3. However, two filled defects levels above the original VBM are found, which are derived from hybridized O *p* and Ti *d* states. Considering these two bands as part of the new valence band (in the case of the $Fe_{2-x}Ti_xO_3$ alloy), the bandgap for the spin-up channel is 1.19 eV, which is much lower than that of pure α-Fe_2O_3: low energy photon absorption will be enhanced.

α-Fe_2O_3:Cr. The Cr ($4s^2 3d^4$) atom in the Cr^{3+} (d^3) ionic charge state in α-Fe_2O_3 can put three *d* electrons in the Cr t_{2d} state and the unoccupied e_d state will be separated to

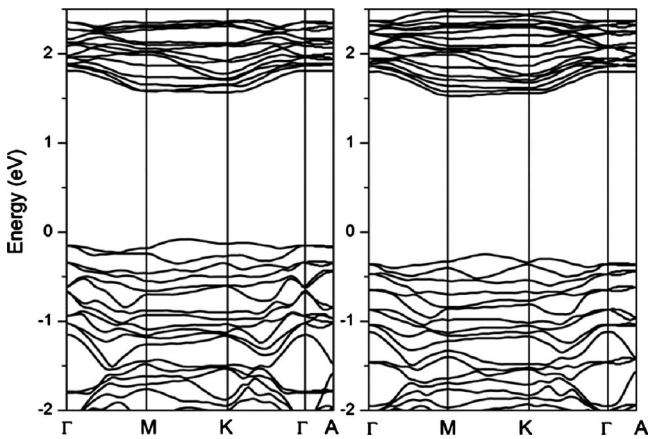

FIG. 3. Calculated electronic band structure for α-Fe_2O_3:Sc. Left panel: spin-up; right panel: spin-down states. The highest occupied state is set to 0 eV.

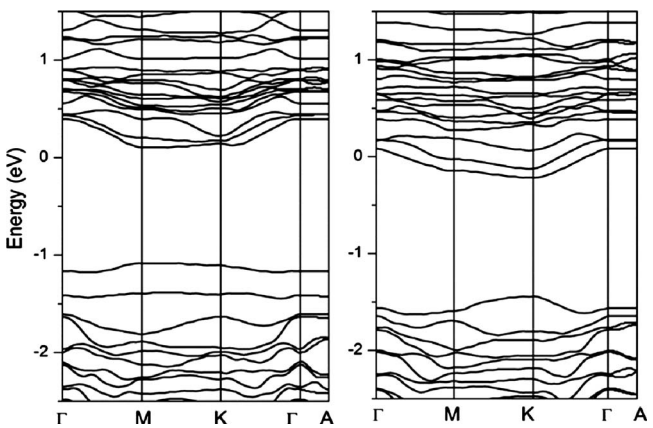

FIG. 4. Calculated electronic band structure for α-Fe_2O_3:Ti. Left panel: spin-up; right panel: spin-down bands. The highest occupied state is set to 0 eV.

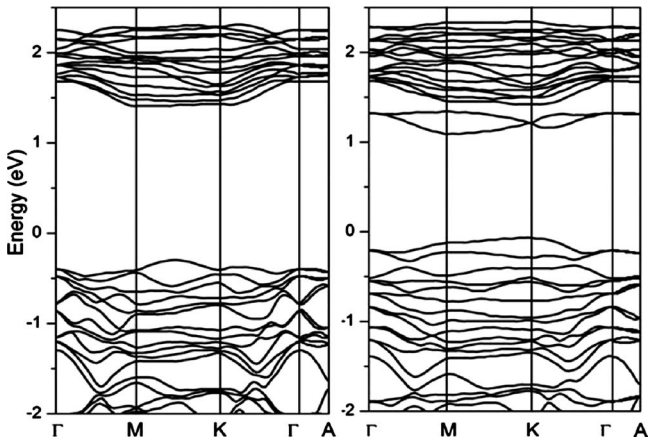

FIG. 5. Calculated electronic band structure for α-Fe_2O_3:Cr. Left panel: spin-up; right panel: spin-down bands. The highest occupied state is set to 0 eV.

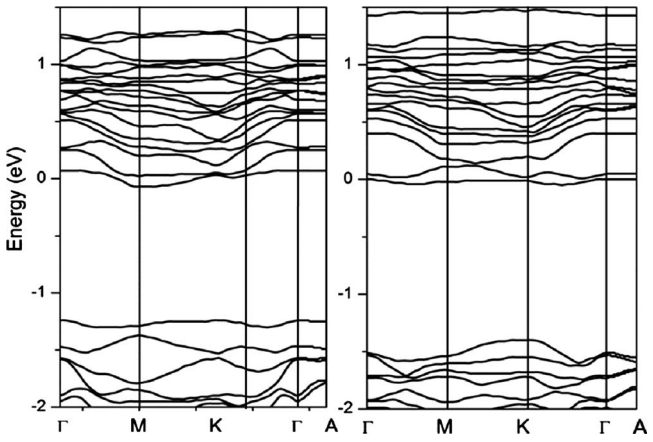

FIG. 6. Calculated electronic band structure for α-Fe_2O_3:Mn. Left panel: spin-up; right panel: spin-down bands. The highest occupied state is set to 0 eV.

higher energies by the octahedral crystal-field splitting. The calculated band structures for spin-up (left panel) and spin down (right panel) of α-Fe_2O_3:Cr are shown in Fig. 5. As discussed above, the bandgap for the spin-up channel is almost the same as that for pure α-Fe_2O_3; but in the spin-down channel, the bandgap (1.17 eV) is much smaller than the pure host due to the strong localization of the occupied spin-down t_{2d} state. The local moment at the Cr site is close to -3 μ_B (replacing an Fe ion of -5 μ_B) and the total moment of the cell is, therefore, 2 μ_B. If the concentration of Cr is increased, i.e., in the alloying regime, these Cr e_d and s orbital derived states will become the bottom of conduction band of $Fe_{2-x}Cr_xO_3$. The new CBM has more dispersion and it could, therefore, enhance the conductivity by improving electron mobility; however, the bandwidth does remain relatively narrow.

α-Fe_2O_3:Mn. Mn ($4s^2 3d^5$) has one more d electron than Cr; thus, when Cr^{3+} is replaced by Mn^{3+} (d^4), part of the spin-down e_d band just below the CBM will become filled. The local magnetic moment of Mn will increase to about -4 μ_B, and the total magnetic moment of the defective cell is reduced to about 1 μ_B. This small total magnetic moment indicates that the spin-splitting between the spin-up and spin-down bands is small, so both CBMs for spin-up and spin-down states are occupied, which renders it as an n-type material. On the other hand, the Mn d band does not contribute much to the VBM. The bandgaps for spin-up and spin down are 1.17 eV and 1.35 eV, respectively. Our calculated band structure for α-Fe_2O_3:Mn, as shown in Fig. 6, is slightly different from the previously published band structure,[28] which shows a partially filled band at the middle of the bandgap. We find that we can also obtain this feature if the volume of the supercell with substitutional Mn was not relaxed. After volume relaxation, this mid-gap partially occupied band splits into filled and empty states deep in the bandgap, which suggests that Mn will be susceptible to oxidation toward Mn^{4+} or reduction toward Mn^{2+}.

α-Fe_2O_3:Ni. Ni ($4s^2 3d^8$) substitution on the spin-down Fe site in α-Fe_2O_3 has a formal Ni^{3+} (d^7) ionic state. The band structures are shown in Fig. 7. Due to large crystal-field splitting, both the spin-up and spin-down Ni t_{2d} states are fully occupied, with the remaining seventh electron occupying one of the spin-down Ni e_d states. Therefore, the local magnetic moment at the Ni site is close to -1 μ_B and the total magnetic moment per cell is 4 μ_B. The spin-down Ni e_d state appears in the middle of the gap; the lower state is fully occupied, whereas, the upper state is empty. This half-filled Ni-derived band in the middle of the bandgap makes α-Fe_2O_3:Ni a good candidate as an intermediate-bandgap material if charge compensation by intrinsic defects (such as oxygen vacancies) to produce the more stable Ni^{2+} species can be avoided. The two states above the VBM in the spin-up channel are also mainly derived from Ni d. Considering these two states as part of a new alloy valence band, the bandgap in the spin-up band structure would be 1.34 eV.

The trend for the incorporation of $3d$ TMs in α-Fe_2O_3 can be further characterized from the DOS plots. Figure 8 shows the total DOS plots for pure α-Fe_2O_3 and α-Fe_2O_3 incorporated with other $3d$ TMs. These DOS plots are aligned with respect to the O $1s$ core level to show the relative shift in the states. Here, it is assumed that the deep O $1s$ level is an appropriate reference energy level, as its actuations due to different dopants in α-Fe_2O_3 can be neglected far from dopant site. The Fermi level, defined as the highest

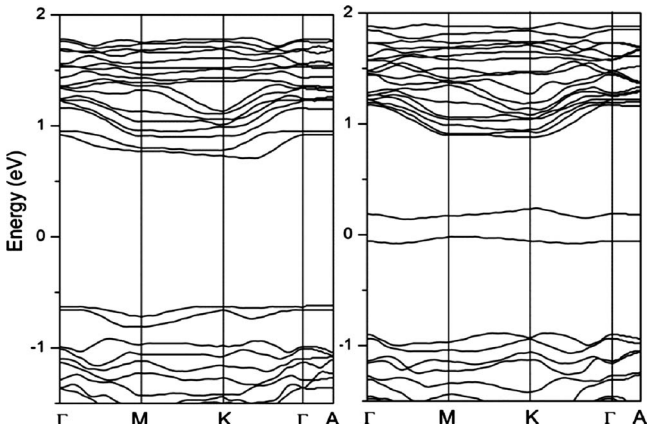

FIG. 7. Calculated electronic band structure for α-Fe_2O_3:Ni. Left panel: spin-up; right panel: spin-down bands. The highest occupied state is set to 0 eV.

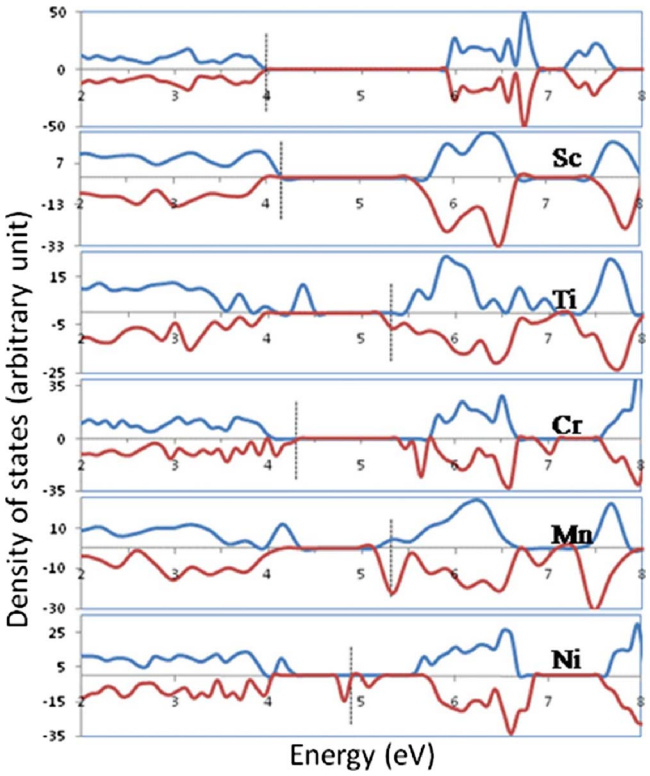

FIG. 8. (Color online) Total electronic DOS plot for pure α-Fe_2O_3 and α-Fe_2O_3 incorporated with Sc, Ti, Cr, Mn, and Ni at substitutional sites. The states are aligned with respect to the O 1*s* core level and the highest occupied state is indicated by the dashed vertical line in each case.

occupied state, is marked by the dashed line in each case. The DOS plots clearly show the trend of the effects of TMs on the electronic structure of α-Fe_2O_3. Whereas the Sc derived band is well mixed with the original conduction band of α-Fe_2O_3, Ni produces two states in the middle of the gap. This trend is consistent with the fact that the *d* orbitals become increasingly localized from Sc to Ni. Among all the considered 3*d* TMs, the Ti and Cr derived bands exhibit the most dispersive features, indicating that the incorporation of Ti and Cr should lead to a lower effective mass for electrons, and, therefore, should somewhat enhance the electrical conductivity.

Further, we find that the incorporation of 3*d* TMs leads to significant volume changes in the defective cell. Except for the larger Sc cation, the incorporation of other TMs results in a volume reduction, as shown in Fig. 9. For Sc substitution, the volume is increased by about 1.4% at the calculated defect concentration. The largest volume reduction (about 2%) was found for Ni substitution, which is related to the strong localization of the Ni *d* orbital. As the dominant contribution of electrical conduction in α-Fe_2O_3 is through small polaron hopping, the volume decrease is likely to aid the conductivity both through a shorter hopping distance and harder phonon frequencies. A recent experimental and theoretical study of group 13 elements doped in α-Fe_2O_3 also showed similar behavior.[29]

It should be mentioned here, that the local distortions created by the TM doping in α-Fe_2O_3 are small due to the low cation size mismatch. For example, for Ti-doped α-Fe_2O_3, the two different local bond angles for O–Ti–O are

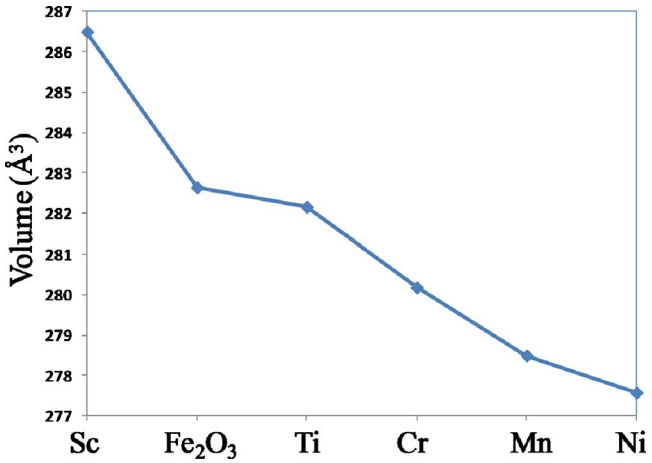

FIG. 9. (Color online) Calculated volumes for defective supercells containing 3*d* TM substitutions in Fe_2O_3. Fe_2O_3 represents pure α-Fe_2O_3.

81.4° and 86.2°, compared to the undoped angles of 78.2° and 86.1°, respectively. On the other hand, the same layer Fe–Fe distances decrease (where the electron hopping mainly takes place); for Ti-doped and undoped cases, the Fe–Fe distances are 2.89 Å and 2.97 Å, respectively. So, in the present case of TM doping, it can be argued that, as the TM dopants are localized in nature and do not inflict much lattice distortion, the local chemical environment for Fe to Fe intralayer hopping sufficiently far from the dopant sites would not change much except for the reduced Fe–Fe distances due to the volume decrement. Therefore, lattice strain, in the form of reduced Fe–Fe distances, may also contribute to improved photon conversion efficiencies in the doped systems, through improved mobility of electrical charge carriers.

It should be pointed out that the incorporation of 3*d* TMs may result in additional effects besides those discussed above. For example, the incorporation of impurities can change the morphology, stoichiometry, crystallinity, and grain size of synthesized materials. The incorporated 3*d* TMs could also favor segregation to the material surface, and some of the 3*d* TMs are potential catalysts for the processes involved in hydrogen and oxygen evolution, which may affect the PEC performance of the synthesized materials. Thus, all possible effects should be considered so that the PEC performance of a material may be evaluated adequately. Nevertheless, the above calculated electronic structure and volume change provide initial insight into the understating how the incorporation of 3*d* TMs may affect the conductivity of α-Fe_2O_3 and lead to the optimization of iron oxide as a cheap visible-light photocatalyst.

IV. CONCLUSIONS

We have studied the properties of α-Fe_2O_3 on the incorporation of substitutional 3*d* TM cations. We have shown that the incorporation of some 3*d* TMs act as electron donors and reduce the effective mass for electrons and hence can promote the electrical conductivity; therefore, it may help to increase the solar-to-hydrogen conversion efficiency by facilitating the separation and transport of photogenerated

charge carriers. Furthermore, we have found that the incorporation of some 3*d* TMs will lead to a net volume reduction, which may affect the polaron hopping probabilities in α-Fe_2O_3. Our results suggest that among all the considered 3*d* TMs, the incorporation of Ti would lead to the greatest increase in electrical conductivity, and, therefore, to the greatest enhancement of PEC performance.

ACKNOWLEDGMENTS

We thank E. McFarland (UCSB) and J. Turner (NREL) for stimulating discussions. The work at NREL is supported by the U.S. Department of Energy under Contract No. DE-AC36-08GO28308.

[1]A. Fujishima and K. Honda, Nature (London) **238**, 37 (1972).
[2]F. E. Osterloh, Chem. Mater. **20**, 35 (2008); A. Kudo and Y. Miseki, Chem. Soc. Rev. **38**, 253 (2009).
[3]A. Walsh, K.-S. Ahn, S. Shet, M. N. Huda, T. G. Deutsch, H. Wang, J. A. Turner, S.-H. Wei, Y. Yan, and M. M. Al-Jassim, Energy Environ. Sci. **2**, 774 (2009).
[4]S. M. Ahmed, J. Leduc, and S. F. Haller, J. Phys. Chem. **92**, 6655 (1988).
[5]A. B. Murphy, P. R. F. Barnes, L. K. Randeniya, I. C. Plumb, I. E. Grey, M. D. Horne, and J. A. Glasscock, Int. J. Hydrogen Energy **31**, 1999 (2006).
[6]A. Kay, I. Cesar, and M. Gratzel, J. Am. Chem. Soc. **128**, 15714 (2006).
[7]K. Itoh and J. O. Bockris, J. Electrochem. Soc. **131**, 1266 (1984).
[8]K. M. Rosso, D. M. A. Smith, and M. Dupuis, J. Chem. Phys. **118**, 6455 (2003).
[9]J. A. Glasscock, P. R. F. Barnes, I. C. Plumb, and N. Savvides, J. Phys. Chem. C **111**, 16477 (2007).
[10]Y. S. Hu, A. Kleiman-Shwarsctein, G. D. Stucky, and E. W. McFarland, Chem. Commun. (Cambridge) **2009**, 2652.
[11]Y. S. Hu, A. Kleiman-Shwarsctein, A. J. Forman, D. Hazen, J. N. Park, and E. McFarland, Chem. Mater. **20**, 3803 (2008).
[12]A. Kleiman-Shwarsctein, Y.-S. Hu, A. J. Forman, G. D. Stucky, and E. W. McFarland, J. Phys. Chem. C **112**, 15900 (2008).
[13]A. Kleiman-Shwarsctein, Y.-S. Hu, G. D. Stucky, and E. W. McFarland, Electrochem. Commun. **11**, 1150 (2009).
[14]W. B. Ingler, J. P. Baltrus, and S. U. M. Khan, J. Am. Chem. Soc. **126**, 10238 (2004).
[15]S. Kumari, C. Tripathi, A. P. Singh, D. Chauhan, R. Shrivastav, S. Dass, and V. R. Satsangi, Curr. Sci. **91**, 1062 (2006).
[16]J. H. Kennedy, M. Anderman, and R. Shinar, J. Electrochem. Soc. **128**, 2371 (1981).
[17]J. P. Perdew and A. Zunger, Phys. Rev. B **23**, 5048 (1981).
[18]P. E. Blöchl, Phys. Rev. B **50**, 17953 (1994).
[19]G. Kresse and D. Joubert, Phys. Rev. B **59**, 1758 (1999).
[20]G. Kresse and J. Hafner, Phys. Rev. B **48**, 13115 (1993); G. Kresse and J. Furthmüller, Comput. Mater. Sci. **6**, 15 (1996); Phys. Rev. B **54**, 11169 (1996).
[21]S. L. Dudarev, G. A. Botton, S. Y. Savrasov, C. J. Humphreys, and A. P. Sutton, Phys. Rev. B **57**, 1505 (1998).
[22]A. Bandyopadhyay, J. Velev, W. H. Butler, S. K. Sarker, and O. Bengone, Phys. Rev. B **69**, 174429 (2004).
[23]G. Rollmann, A. Rohrbach, P. Entel, and J. Hafner, Phys. Rev. B **69**, 165107 (2004).
[24]J. Lielmezs and A. C. D. Chaklader, J. Appl. Phys. **36**, 866 (1965).
[25]N. Iordanova, M. Dupuis, and K. M. Russo, J. Chem. Phys. **122**, 144305 (2005).
[26]L. Pauling, *The Nature of the Chemical Bond* (Cornell University Press, Ithaca, 1939).
[27]Y. Xu and M. A. A. Schoonen, Am. Min. **85**, 543 (2000).
[28]J. Velev, A. Bandyopadhyay, W. H. Butler, and S. Sarker, Phys. Rev. B **71**, 205208 (2005).
[29]A. K. Shwarsctein, M. N. Huda, A. Walsh, Y. Yan, G. D. Stucky, Y.-S. Hu, M. M. Al-Jassim, and E. W. McFarland, Chem. Mater. **22**, 510517 (2010).